RECENT PROGRESS IN HIGH-GAIN FEL THEORY

Zhirong Huang*
Stanford Linear Accelerator Center,
Stanford, CA 94309, USA

Abstract

High-gain free electron lasers (FEL) are being developed as extremely bright x-ray sources of a next-generation radiation facility. In this paper, we review the basic theory and the recent progress in understanding the startup, the exponential growth and the saturation of the high-gain process, emphasizing the self-amplified spontaneous emission (SASE). We will also discuss how the FEL performance may be affected by various errors and wakefield effects in the undulator.

INTRODUCTION

Free electron lasers (FEL) hold great promises as tunable-wavelength, high-power coherent radiation sources. In the x-ray wavelength range (from a few nm down to 1 Angstrom or below) where no quantum laser exists, a high-gain FEL operated in the self-amplified spontaneous emission (SASE) mode can in principle generate multi-gigawatts and femtosecond coherent x-ray pulses. Tremendous progress in accelerator and FEL technologies has been made in past years towards such a "fourth-generation" radiation facility, demonstrated by the successful SASE FEL experiments at visible and ultraviolet wavelengths [1, 2, 3]. As a result of intense R&D, several x-ray FEL projects are either under construction or being proposed (see, e.g., Refs. [4, 5, 6]). This paper reviews the recent progress in understanding high-gain FELs in general and SASE FELs in particular.

BASIC CONSIDERATIONS

Despite the fact that the first FEL theory is based on a quantum mechanical analysis [7], all operating and proposed FEL devices can be adequately described by the classical theory. The quantum recoil is insignificant as the ratio of the photon energy to the electron energy is usually much smaller than the FEL gain bandwidth (typically on the order of 10^{-2} to 10^{-3}). The quantum effect may be important when an extremely bright and low-energy electron beam interacts with an energetic photon pulse in a laser undulator. This regime has been studied recently in Ref. [8].

The electrons wiggle in the periodic magnetic field created by an undulator can resonantly exchange energy with an external radiation or with the spontaneous emission of these electrons. The resonant condition for the fundamental undulator radiation (i.e., the first harmonic) is

$$\lambda_1 = \frac{\lambda_u}{2\gamma_0^2}\left(1+\frac{K_0^2}{2}\right) = \frac{2\pi}{k_1} = \frac{2\pi c}{\omega_1}\,, \qquad (1)$$

where $K_0 = 0.94 B_0[\text{Tesla}]\lambda_u[\text{cm}]$ is the dimensionless undulator strength parameter, B_0 is the peak magnetic field, $\lambda_u = 2\pi/k_u$ is the undulator period, and $\gamma_0 mc^2$ is the average electron energy. For a sufficiently bright electron beam and/or a sufficiently long undulator, this resonant interaction leads to an exponential growth of the radiation power until it reaches a saturation level. A very important scaling parameter for a high-gain FEL is the Pierce parameter ρ defined by [9]

$$\rho = \left[\frac{K_0^2[\text{JJ}]^2}{32}\frac{k_p^2}{k_u^2}\right]^{1/3} = \left[\frac{1}{16}\frac{I_e}{I_A}\frac{K_0^2[\text{JJ}]^2}{\gamma_0^3\sigma_x^2 k_u^2}\right]^{1/3}\,, \qquad (2)$$

where the Bessel function factor [JJ]=$J_0(\xi) - J_1(\xi)$ with $\xi = K_0^2/(4+2K_0^2)$ for a planar undulator, $k_p = \sqrt{2I_e/(\gamma_0^3 I_A \sigma_x^2)}$ is the longitudinal plasma oscillation wavenumber, I_e is the electron peak current, $I_A \approx 17$ kA is the Alfvén current, and σ_x is the rms transverse size of the electron beam. For instance, the electric field amplitude gain length is approximately $L_g = (2\rho k_u)^{-1} = \lambda_u/(4\pi\rho)$, the relative FEL bandwidth at saturation is close to ρ, and the saturation power is about ρ times the electron beam power.

As the current density of the electrons is modulated by the FEL interaction around the resonant wavelength λ_1, the longitudinal space charge force between electrons tends to counteract the bunching action if the reduced plasma oscillation wavelength k_p^{-1} is comparable to the FEL gain length $L_g = (2\rho k_u)^{-1}$. Examination of Eq. (2) for $K \sim 1$ shows that this condition requires that $k_p \to k_u$ and that $\rho \to 1$. In typical short-wavelength FELs using high-energy electron beams, $\rho \sim 10^{-3}$, hence we can neglect self-interactions of the electron beam around the FEL resonant frequency and focus on beam-radiation interaction.

The beam-radiation interaction occurs in a vacuum pipe (or an in-vacuum undulator structure). The presence of a metallic surface may modify characteristics of both the radiation and the electron beam. In fact, the first SASE FEL operating in the millimeter wavelength region employed a waveguide to confine the radiation against diffraction [10]. For a high-gain FEL at visible or shorter wavelengths, the transverse size of the radiation is usually much smaller than the pipe radius. Thus, we can neglect the boundary condition on the transverse radiation mode. Nevertheless, the interaction of the vacuum pipe with the high-current electron

* zrh@slac.stanford.edu

beam creates a wakefield that changes the beam properties along the bunch. Effects of the wakefield on the FEL interaction may be significant for x-ray FELs employing long undulator systems and will be discussed in this paper.

OVERVIEW OF HIGH-GAIN THEORY

FEL pendulum equations

In the so-called ponderomotive potential of the combined undulator and radiation fields, the longitudinal electron motion can be described by a relative energy variable $\eta = (\gamma - \gamma_0)/\gamma_0 \ll 1$ and a ponderomotive phase variable $\theta = (k_1 + k_u)z - \omega_1 t^*$, where $ct^*(z)$ is the undulator-period-averaged electron arrival time at the undulator distance z. The rate of the energy exchange with a transverse radiation field is

$$\frac{d\eta}{dz} = \frac{eK_0[\mathrm{JJ}]}{4\gamma_0^2 mc^2} \int d\omega E_\omega(\mathbf{x}; z) e^{i\omega\theta/\omega_1} + \text{c. c.}\,, \quad (3)$$

where E_ω is the transverse radiation field (at a frequency $\omega \sim \omega_1$) that is slowly varying in z, $\mathbf{x} = (x, y)$ represents the transverse coordinates, and c. c. stands for complex conjugate. The rate of the ponderomotive phase change is

$$\frac{d\theta}{dz} = k_1 + k_u - \frac{k_1}{\beta_\parallel} = k_u - k_1 \frac{1 + K_0^2/2}{2\gamma^2} - \frac{k_1}{2}\beta_\perp^2\,, \quad (4)$$

where $c\beta_\parallel$ is the average longitudinal velocity, and $c\beta_\perp$ is the transverse velocity due to the betatron motion. In the absence of any betatron motion (when $\beta_\perp = 0$), inserting the resonant condition Eq. (1) into Eq. (4) yields

$$\frac{d\theta}{dz} = 2k_u\eta\,. \quad (5)$$

Equations (3) and (5) are recognized as the FEL pendulum equations [11]. An initially unbunched beam in the ponderomotive potential develops an energy modulation at the radiation wavelength. The energy modulation is turned into a current modulation that leads to exponential amplification of the radiation field in a long undulator.

Since the FEL interaction is a resonant energy exchange between the electron and the radiation field, the evolution of electrons' ponderomotive phase may affect the FEL performance critically. For example, the betatron motion of a finite-emittance beam introduces an intrinsic phase spread through $\beta_\perp$ for the electrons at the same longitudinal position. A deviation of the undulator parameter K from the design value and a change in electron beam energy due to wakefield effects can also change the ponderomotive phase along the undulator distance. The effects of beam qualities on the FEL performance will be discussed next, while the effects of undulator qualities and wakefield will be discussed in the following section.

Solutions in the small signal regime

For a high-gain FEL, the equations of motion for an electron beam must be solved together with the Maxwell equation for the radiation field. In the small signal regime before saturation, the FEL equations are solved in the one-dimensional (1-D) case taking into account the SASE start-up from shot noise in the electron beam [12, 13]. Three-dimensional (3-D) diffraction effects can be included using Moore's guided modes [14] and can be extended to the SASE case [15, 16]. In general, the radiation field can be written as

$$E_\omega(\mathbf{x}; z) = \sum_n C_n E_n(\mathbf{x}) e^{-i\mu_n 2\rho k_u z}\,, \quad (6)$$

where E_n describe the transverse profile of the n^{th} eigenmode, μ_n is the complex growth rate corresponding to this eigenmode, and C_n is the mode expansion coefficient found by solving the initial value problem. In the high-gain regime a Gaussian-like fundamental mode with the largest growth rate (largest $\mathrm{Im}\mu_0$) dominates over other higher-order modes, i.e.,

$$E_\omega(\mathbf{x}; z) \approx C_0 E_0(\mathbf{x}) e^{-i\mu_0 2\rho k_u z} \quad \text{when } 2\rho k_u z \gg 1\,. \quad (7)$$

Thus, the transverse profile of the radiation appears to be frozen with an exponentially growing amplitude.

One of the most important FEL design parameters is the power gain length of the fundamental mode given by

$$L_G = \frac{\lambda_u}{8(\mathrm{Im}\mu_0)\pi\rho} \equiv L_{G0}(1 + \Lambda)\,, \quad (8)$$

where $L_{G0} = \lambda_u/(4\sqrt{3}\pi\rho)$ is the 1-D power gain length of a monoenergetic beam. Taking into account beam energy spread, emittance and focusing, as well as radiation diffraction and guiding, a universal scaling function and an approximate variational solution for L_G is obtained in Ref. [17]. Based on numerical studies of the FEL eigenmode equation, Xie obtains a very useful fitting formula for Λ (and hence L_G) at the optimal frequency as [18, 19]:

$$\begin{aligned}\Lambda =& a_1\eta_d^{a_2} + a_3\eta_\varepsilon^{a_4} + a_5\eta_\gamma^{a_6} + a_7\eta_\varepsilon^{a_8}\eta_\gamma^{a_9} \\ &+ a_{10}\eta_d^{a_{11}}\eta_\gamma^{a_{12}} + a_{13}\eta_d^{a_{14}}\eta_\varepsilon^{a_{15}} + a_{16}\eta_d^{a_{17}}\eta_\varepsilon^{a_{18}}\eta_\gamma^{a_{19}}\,.\end{aligned} \quad (9)$$

Here the three scaled parameters are

$$\begin{aligned}\eta_d =& \frac{L_{G0}}{2k_1\sigma_x^2} \quad \text{(diffraction parameter)}\,, \\ \eta_\varepsilon =& \frac{L_{G0}}{\bar{\beta}} \frac{\varepsilon}{\lambda_1/(4\pi)} \quad \text{(angular spread parameter)}\,, \\ \eta_\gamma =& 4\pi \frac{L_{G0}}{\lambda_u}\sigma_\delta \quad \text{(energy spread parameter)}\,, \end{aligned} \quad (10)$$

where ε is the rms transverse emittance, $\bar{\beta}$ is the average beta function, and σ_δ is the relative rms energy spread. The fitting coefficients are

$$\begin{aligned}&a_1 = 0.45\,, a_2 = 0.57\,, a_3 = 0.55\,, a_4 = 1.6\,, a_5 = 3\,, \\ &a_6 = 2\,, a_7 = 0.35\,, a_8 = 2.9\,, a_9 = 2.4\,, a_{10} = 51\,, \\ &a_{11} = 0.95\,, a_{12} = 3\,, a_{13} = 5.4\,, a_{14} = 0.7\,, a_{15} = 1.9\,, \\ &a_{16} = 1140\,, a_{17} = 2.2\,, a_{18} = 2.9\,, a_{19} = 3.2\,. \end{aligned} \quad (11)$$

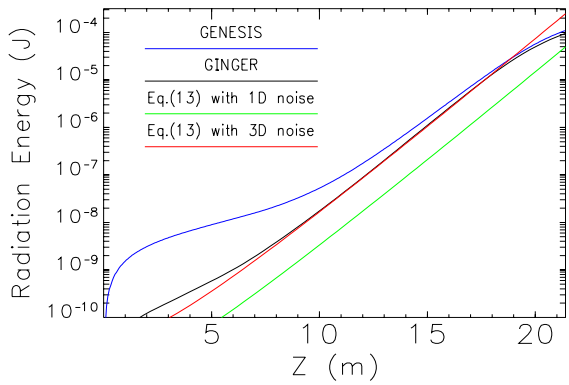

Figure 1: GINGER (black) and GENESIS (blue) simulations of the LEUTL FEL energy at 130 nm versus the undulator distance z, as compared from predictions of Eq. (13) with 3-D noise (red) and 1-D noise (green).

The discrepancy between Xie's fitting formula and numerical solutions of the FEL eigenmode equation is typically less than 10%. These positive coefficients show that all three scaled beam parameters in Eq. (10) should be kept small to avoid a large gain reduction, corresponding to the well-known requirements for the beam quality.

Including the frequency-dependence of the complex growth rate in Eq. (7) and integrating over the transverse coordinates, we obtain the FEL power spectrum in the high-gain regime as

$$\frac{dP}{d\omega} = g_A \left(\frac{dP_0}{d\omega} + g_S \frac{\rho\gamma_0 mc^2}{2\pi} \right) \exp\left(\frac{z}{L_G} - \frac{\Delta\omega^2}{2\sigma_\omega^2} \right), \tag{12}$$

where $dP_0/d\omega$ is the input power spectrum, $\rho\gamma_0 mc^2/(2\pi)$ is the 1-D SASE noise power spectrum [15] and can be interpreted as the spontaneous undulator radiation in the first two power gain length [20], and σ_ω is the SASE bandwidth that decreases with z up to the FEL saturation point (with a typical value $\rho\omega_1$). g_A and g_S determine the input coupling to the fundamental mode and the effective noise in units of $\rho\gamma_0 mc^2/(2\pi)$, respectively. $g_A = 1/9$ and $g_S = 1$ in the 1-D, cold beam limit [12, 13] and are computed for a general beam distribution in 3-D in Refs. [21, 22]. Integrating the SASE term over the frequency, we have the average SASE power as

$$P = g_A P_n \exp\left(\frac{z}{L_G} \right). \tag{13}$$

Here $P_n = g_S \rho\gamma_0 mc^2 \sigma_\omega/\sqrt{2\pi}$ is the effective noise power for SASE. The agreement between time-dependent SASE simulations using GINGER [23] and GENESIS [24] and Eq. (13) are very good when the proper input coupling coefficient and effective noise power (i.e., g_A and g_S) are calculated, as shown in Fig. 1 for the LEUTL FEL [1] at $\lambda_1 = 130$ nm. Note that GENESIS is a 3-D code that do not assume azimuthal symmetry in the radiation profile and hence excite many more higher-order modes in the start-up regime.

Transverse coherence and mode size

Since the fundamental transverse mode possesses the largest growth rate and dominates over other higher order modes with smaller growth rates in the high-gain regime, the SASE FEL can reach almost full transverse coherence before saturation, even when the emittance of the electron beam is larger than the diffraction-limited radiation emittance $\lambda_1/(4\pi)$ as found in most current x-ray FEL designs. The frequency-dependency of the fundamental mode within the finite SASE bandwidth introduces a small increase of the radiation emittance [25, 26], which is negligible for x-ray FELs.

In general, the transverse mode size (and angular divergence) requires numerical solutions of the FEL eigenmode equation. Two simple limiting cases can be discussed here. In the large e-beam cross section limit assuming that the electron microbunching is more or less uniform along the transverse directions, the transverse profile of the radiation field is proportional to the transverse profile of the electron density. Thus, the rms spot size of the radiation intensity is about $\sqrt{2}$ smaller than the rms transverse size of the electron beam [27]. This is typically the case for an x-ray FEL such as the LCLS with the electron emittance larger than the radiation emittance. On the other hand, in a visible or infrared-wavelength FEL using electron beams with emittance smaller than the radiation emittance, the radiation mode size tends to be larger than the electron transverse size due to the diffraction effect. In this small e-beam cross section limit, the rms spot size of the radiation is independent of the e-beam size and can be estimated as

$$\sigma_r \approx \sqrt{\frac{\lambda_1}{4\pi} 2L_G^D}, \quad \text{where} \quad L_G^D \approx \frac{\lambda_u}{4\pi} \sqrt{\frac{\gamma_0 I_A}{I_e} \frac{1 + K_0^2/2}{K_0^2 [\mathrm{JJ}]^2}}$$

is the power gain length in the diffraction-dominated regime [17].

Temporal characteristics

Due to the noisy startup, the temporal property of a SASE FEL is that of a chaotic light [28, 29, 30]. In the time-domain a SASE pulse of duration T consists of $M = T/\tau_c$ independent spikes (modes), characterized by the coherence time [29, 30]

$$\tau_c = \frac{\sqrt{\pi}}{\sigma_\omega}. \tag{14}$$

For an x-ray FEL at $\lambda_1 \approx 1$ Å, the coherence time can be as short as a few hundred attoseconds, opening up the possibility of selecting a single attosecond spike for the ultra-fast scientific applications (see, e.g., Refs. [31, 32]). The intensity of each temporal spike fluctuates 100% for a transversely coherent radiation.

The full SASE spectral width is about $2\sqrt{\pi}\sigma_\omega$, consisting of also M independent modes. Each frequency mode is characterized by the spectral coherence range $2\pi/T$ and its intensity also fluctuates 100%. Integrating the intensity

over time or frequency, the statistical fluctuation of the total radiated energy is reduced by $\sqrt{M}$, which is usually a large factor for an x-ray SASE FEL.

For a frequency-chirped SASE generated by an energy-chirped electron beam, the coherence time is independent of the chirp as long as the frequency span within a temporal spike is smaller than its bandwidth, while the spectral coherence range increases linearly with the chirp [33]. A narrow-bandwidth monochromator may be used to select a much shorter section of the chirped x-ray pulse (see, e.g., Ref. [34]).

Nonlinear harmonic generation

The FEL interaction introduces both energy and density modulations (microbunching) of the electron beam. Before saturation strong bunching at the fundamental frequency ω_1 produces rich harmonic bunching and significant harmonic radiation in a planar undulator [35, 36]. A 3-D analysis of nonlinear harmonic generation [37] shows that the gain length, transverse and temporal properties of the first few harmonics are eventually governed by those of the fundamental after a certain stage of exponential growth. For example, driven by the third power of the radiation field in the fundamental, the third nonlinear harmonic grows three times faster, has an equally coherent transverse mode (with a smaller spot size), and has a more spiky temporal structure than the fundamental radiation of a SASE FEL. The more pronounced temporal spikes of these nonlinear harmonic radiation may enable selections of a shorter temporal pulse with the highest intensity [38]. As a numerical example, Ref. [37] calculates the third harmonic power (at 0.5 Å) of the LCLS can reach almost 1% of its fundamental power at 1.5 Å, extending the wavelength reach of this x-ray source. The power of the second-harmonic radiation is much reduced for x-ray FELs but may still be significant for long-wavelength FELs using relatively low-energy electron beams [39, 3].

Saturation

Together with the development of the microbunching, the energy spread of the electron beam increases and eventually stops the exponential growth, and the FEL reaches saturation at about $z_{\rm sat} \approx \lambda_u/\rho \approx 20L_G$ for a typical SASE FEL. The effect of energy spreading can be included using a quasi-linear approximation that determines the saturation power [40], which agrees reasonably with a simulation fitting formula given by [18]

$$P_{\rm sat} \approx 1.6\left(\frac{L_{G0}}{L_G}\right)^2 \rho P_{\rm beam} = \frac{1.6}{(1+\Lambda)^2}\rho P_{\rm beam}\,, \quad (15)$$

where Λ is defined in Eq. (8), and $P_{\rm beam}[{\rm GW}] = (\gamma_0 mc^2/e)[{\rm GV}]I_e[{\rm A}]$ is the total electron beam power.

The radiation characteristics after saturation are more complex, especially for SASE FELs. The FEL bandwidth starts to increase due to the appearance of sidebands associated with synchrotron oscillations of electrons trapped in the ponderomotive potential [41]. In general both the transverse and the temporal coherence decrease with the undulator distance in the saturation regime. Although the fluctuation of the total radiated energy is also reduced after saturation, the fluctuation of a single frequency mode filtered by a monochromator is still 100% just as in the exponential growth regime [29]. An analytical model that reproduces such a statistical fluctuation in the early saturation regime is recently developed in Ref. [42].

UNDULATOR ERRORS AND WAKEFIELDS

The design of a typical x-ray FEL calls for a small-gap undulator system of about a hundred meter in length. For technical feasibility, the long undulator beam line is divided into many undulator segments and beam focusing/diagnostic sections. Errors in undulator field qualities and electron beam steering can degrade the FEL performance. In addition to these errors, wakefields induced by a high-current beam in the small-gap vacuum chamber can also interfere with the FEL gain process. In this section, we discuss how the FEL theory may be applied to study these effects.

Undulator errors

We will assume that each undulator segment is shimmed to have vanishing first and second magnetic field integrals (no net steering errors) and focus on the variations of the undulator parameter K due to magnetic field errors or transverse misalignments among segments (since K is a function of transverse coordinates). Using the 1-D FEL equations, Yu et al. [43] study the effect of undulator errors on the ponderomotive phase, which can be obtained from Eq. (4):

$$\begin{aligned}\frac{d\theta}{dz} =& k_u - k_1\frac{1+(K_0+\Delta K)^2/2}{2\gamma^2}\\ \approx& 2k_u\eta - k_u\frac{K_0\Delta K(z)}{1+K_0^2/2}\,.\end{aligned} \quad (16)$$

Here the first term describes the usual pendulum motion, and the second term determines the amount of the phase kick due to small changes in K. For undulator errors, we can model $\Delta K(z) = \Delta K_n$ for $(n-1)L_c < z < nL_c$ $(n = 1, 2, 3, ...)$, where ΔK_n is a random quantity with $\langle \Delta K_n\rangle = 0$ and the correlation length $L_c = N_c\lambda_u$ is assumed to be much shorter than the approximate field gain length $L_g = \lambda_u/(4\pi\rho)$. Then the net phase shift per gain length is

$$\delta\theta = \sum_{n=1}^{L_g/L_c} N_c\frac{2\pi K_0\Delta K_n}{1+K_0^2/2}\,. \quad (17)$$

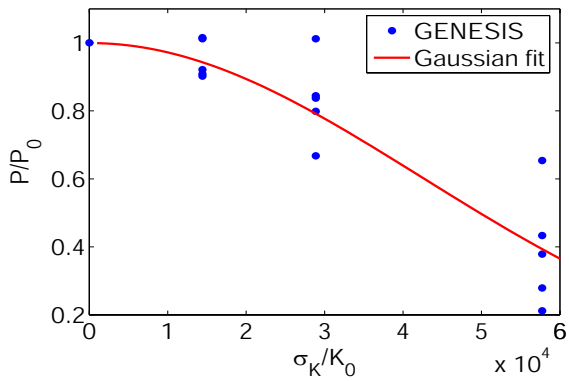

Figure 2: Power degradation factor P/P_0 at FEL saturation versus σ_K/K_0 in the LCLS 33 undulator segments. Here σ_K is the rms value of a uniform segment $\bar{K}$ error distribution. Five random error distributions are used for a given σ_K. The rms width of the Gaussian fit is 4.2×10^{-4}.

For $L_g/L_c \gg 1$, $\delta\theta$ has a zero mean and a variance

$$W = \overline{\delta\theta^2} = \frac{L_g}{L_c}\left(N_c \frac{2\pi K_0^2}{1+K_0^2/2}\frac{\sigma_K}{K_0}\right)^2 = \frac{\pi N_c K_0^4}{(1+K_0^2/2)^2}\frac{(\sigma_K/K_0)^2}{\rho} \approx 4\pi N_c \frac{(\sigma_K/K_0)^2}{\rho}\,. \tag{18}$$

A perturbation analysis yields the radiation power as [43]

$$P \approx P_0 \exp\left(-\frac{2W}{9}\frac{z}{L_g}\right)\,, \tag{19}$$

where P_0 is the power without errors.

For a negligible power degradation near the SASE saturation at $z \approx 10L_g$, the mean square of the ponderomotive phase shift per gain length $W \ll 1$. For errors associated with magnetic pole field B_0 that may occur every undulator period, $N_c \sim 1$, then we have [43]

$$\frac{\sigma_{B_0}}{B_0} < \sqrt{\frac{\rho}{4\pi}}\,. \tag{20}$$

Hence the pole field error tolerance is quite relaxed because it scales as $\sqrt{\rho}$ instead of ρ. On the other hand, if the length of the undulator segment is a significant fraction of L_g as in the LCLS case, the error in the average undulator parameter $\bar{K}$ per segment is now correlated over $N_c \to (4\pi\rho)^{-1}$. Although the perturbation analysis is not strictly valid in this case, Eq. (18) suggests that the error tolerance for $\bar{K}$ is

$$\frac{\sigma_K}{K_0} < \rho\,. \tag{21}$$

The LCLS has the FEL parameter $\rho \approx 5 \times 10^{-4}$ and 33 undulator segments (each with 3.4 m in length) [4]. Figure 2 shows that the GENESIS SASE simulation results for the LCLS undulator segment $\bar{K}$ errors is in qualitative agreement with the requirement of Eq. (21).

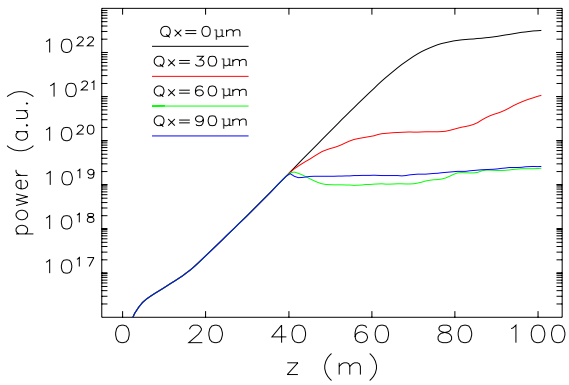

Figure 3: GENESIS simuluation of the LCLS far-field power for various quadrupole offsets Q_x at $z = 40$ m.

Beam trajectory errors

The effects of non-straight beam trajectory may be illustrated with a heuristic 3-D model when an microbunched beam is kicked by an error dipole field (e.g., a misaligned quadrupole) [44]. While the direction of the beam trajectory changes after the kick by a deflecting angle ϕ, the wavefront orientation normal to the microbunching plane does not. This discrepancy results in two mechanisms for gain degradation: a decrease in coherent radiation efficiency and an increased smearing of microbunching due to the intrinsic angular spread. Both mechanisms are characterized by a critical angle [44]

$$\phi_c = \sqrt{\frac{\lambda_1}{L_G}} \tag{22}$$

as the power gain length after the kick becomes approximately $L_G/(1-\phi^2/\phi_c^2)$. In the LCLS case, $\phi_c \approx 6$ μrad at $\lambda_1 = 1.5$ Å for $L_G \approx 4$ m. For quadrupoles equally spaced among the LCLS undulator segments, the rms trajectory angle should be controlled to within 1 μrad in order to guarantee a negligible gain reduction.

Since a sufficient trajectory distortion can destroy the FEL interaction, kicking the beam at selected undulator locations may facilitate the z-dependent FEL power measurements using a single diagnostic station at the end of the undulator beam line. This technique is especially useful when intra-undulator FEL diagnostic stations become difficult. We study this trajectory distortion method for the LCLS z-dependent power measurement with GENESIS simulations. For a quadrupole with a focal length $f = 10$ m, a small horizontal offset $Q_x = 60$ μm corresponds to a kick angle $\phi = Q_x/f = \phi_c$. Figure 3 shows that a quadrupole at $z = 40$ m with a horizontal offset $Q_x \geq 60$ μm (i.e., a kick angle $\phi \geq \phi_c$) inhibits further growth of the FEL fundamental mode, producing an approximately constant on-axis radiation intensity which may be detected by a far-field x-ray diagnostic station after the undulator. Similar conclusions hold at other undulator locations in the exponential growth regime.

Wakefield effects

As mentioned earlier, a high-current electron bunch induces a short-range wakefield that changes the beam properties in the long undulator line. For the LCLS, the dominant (longitudinal) wakefield is caused by the resistive wall of the vacuum pipe [45] and creates an energy variation along the undulator distance as well as along the bunch position. Since the typical bunch length for an x-ray FEL greatly exceeds the radiation slippage length over the entire undulator, the energy variation within an FEL slippage length (known as an FEL slice) is usually negligible for the wakefield that do not vary rapidly inside the bunch. Thus, the main effect of the undulator wakefield is due to a significant energy variation along the undulator distance and is equivalent to that caused by tapering the undulator parameter for a particular FEL slice. The last point can be shown by rewriting the phase Eq. (4) as

$$\frac{d\theta}{dz} = 2k_u \Big[\underbrace{\frac{\gamma(z)-\gamma_c(z)}{\gamma_0}}_{\equiv \eta} + \underbrace{\frac{\gamma_c(z)-\gamma_0}{\gamma_0}}_{\equiv \delta} \Big], \qquad (23)$$

where $\eta(z)$ is now the energy deviation from the beam central energy $\gamma_c mc^2$ and is still governed by Eq. (5) due to the FEL interaction, and $\delta(z)$ is the wakefield-induced energy change relative to the initial energy $\gamma_0 mc^2$ for this FEL slice. Equation (23) is the same as Eq. (16) if

$$\delta(z) = -\frac{K_0 \Delta K(z)}{(2+K_0^2)} \approx -\frac{\Delta K(z)}{K_0}, \quad \text{for } K_0^2 \gg 2. \quad (24)$$

Note that δ here is not a randomly fluctuating quantity as was the case for undulator errors. Instead, δ is a linear function of z for wakefield induced energy change or a linear taper of the undulator parameter.

In general $\delta(z)$ is not small but can be considered as slowly varying if the fractional energy change per field gain length is less than ρ. In the small signal regime before saturation, the WKB approximation can be used to solve the FEL equations and to obtain the SASE power as [46]

$$P(z) \approx P_m(z) \exp\left[-\frac{1}{2} \left(\frac{\delta(z)-\delta_m(z)}{\sqrt{3}\sigma_\omega(z)/\omega_1} \right)^2 \right], \qquad (25)$$

where P_m is the maximum power at the optimal energy change δ_m or an equivalent undulator taper. For the LCLS, a fractional energy increase of 2ρ over the saturation distance $z_{\rm sat} \approx 90$ m improves the saturation power by about a factor of 2 as compared to the nominal saturation power without any external energy change or taper (e.g., that given by Eq. (15) or FEL simulations in absence of wakefield and taper). Since the FEL bandwidth $\sigma_\omega(z_{\rm sat})/\omega_1$ is close to ρ, Eq. (25) indicates that the SASE power has a FWHM in $\delta \approx 4\rho$ at saturation.

For a given wake energy variation as a function of the bunch coordinate, Eq. (25) can be used to obtain the FEL power along the bunch position and to yield the average SASE power over the bunch. As a numerical example, Ref. [46] considers a sinusoidal energy oscillation that resembles the resistive wall wakefield in the core part of the 1-nC-charge LCLS bunch [45]. Figure 4 shows the average power degradation factor (with respect to the maximum power P_m) as a function of the fractional energy oscillation amplitude δ_A with and without a linear taper that yields $\delta_m = 2\rho$ over $z_{\rm sat}$. For a round 5-mm-diameter vacuum pipe, $\delta_A \approx 6\rho$ for Cu and 3ρ for Al at $z_{\rm sat} = 90$ m, then the average power in this part of the bunch is about 50 % (25 %) of P_m for Cu (Al) vacuum pipe, insensitive to the undulator taper for large energy oscillation amplitudes as shown in Fig. 4. To take advantage of the power enhancement due to the above taper, a 200-pC-charge bunch configuration with a much reduced wakefield amplitude is studied for the LCLS [47]. The FEL simulation results are found to agree with the theoretical prediction.

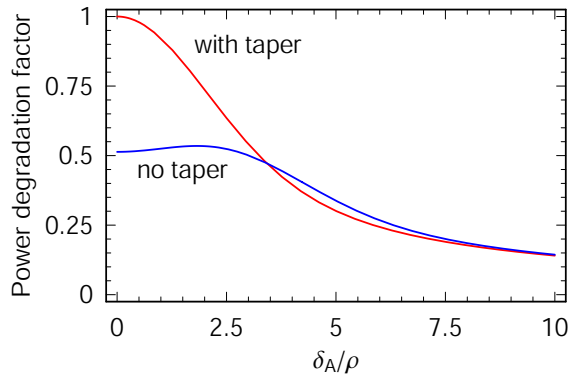

Figure 4: Power degradation factor averaged over the core part of the bunch (with about 30 μm in length) versus the sinusoidal wake oscillation amplitude δ_A/ρ at the LCLS saturation ($z = 90$ m) for a prescribed tapered undulator (in red) and without any taper (in blue) (from Ref. [46]).

CONCLUSIONS

This paper reviews the recent progress in understanding and quantifying the high-gain FEL behaviors in both ideal and more realistic accelerator environment. These theoretical models provide physical pictures, benchmark simulation codes, and guide the FEL designs and experiments. The intense efforts in realizing x-ray FELs and enhancing their performance will stimulate further theoretical developments in this area.

ACKNOWLEDGMENTS

This paper is dedicated to the memory of the late scientist Ming Xie (1959-2004). The author benefits from stimulating discussions with many colleagues including Ming Xie. The author also wishes to thank Kwang-Je Kim for his insight and guidance on many topics discussed here. This work is supported by the U.S. Department of Energy contract DE-AC02-76SF00515.

REFERENCES

[1] S. Milton *et al.*, Science **292**, 2037 (2001).

[2] V. Ayvazyan *et al.*, Phys. Rev. Lett. **88**, 104802-1 (2002).

[3] A. Tremaine *et al.*, Phys. Rev. Lett. **88**, 204801-1 (2002).

[4] Linac Coherent Light Source Conceptual Design Report, SLAC-R-593, SLAC (2002).

[5] TESLA XFEL Technical Design Report, TESLA FEL 2002-09, DESY (2002).

[6] SPring-8 Compact SASE Source Conceptual Design Report, http://www-xfel.spring8.or.jp/, SPring-8 (2005).

[7] J. Madey, J. Appl. Phys. **42**, 1906 (1971).

[8] R. Bonifacio, N. Piovella, and G. Robb, Nucl. Instrum. Methods Phys. Res. A **543**, 645 (2005).

[9] R. Bonifacio, C. Pellegrini, and L. Narducci, Opt. Commun. **50**, 373 (1984).

[10] T. J. Orzechowski, B. Anderson, W. M. Fawley, D. Prosnitz, E. T. Scharlemann, and S. Yarema, Phys. Rev. Lett. **54**, 889 (1985).

[11] W. Colson, Phys. Lett. **64**, 190 (1977).

[12] K.-J. Kim, Nucl. Instrum. Methods Phys. Res., Sect. A **250**, 396 (1986a).

[13] J.-M. Wang and L.-H. Yu, Nucl. Instrum. Methods Phys. Res., Sect. A **250**, 484 (1986).

[14] G. Moore, Opt. Commun. **52**, 46 (1984).

[15] K.-J. Kim, Phys. Rev. Lett. **57**, 1871 (1986b).

[16] S. Krinsky and L.-H. Yu, Phys. Rev. A **35**, 3406 (1987).

[17] L.-H. Yu, S. Krinsky, and R. Gluckstern, Phys. Rev. Lett. **64**, 3011 (1990).

[18] M. Xie, in *Proceedings of the 1995 Particle Accelerator Conference* (IEEE, Piscataway, NJ, 1995), p. 183.

[19] M. Xie, Nucl. Instrum. Methods Phys. Res., Sect. A **445**, 59 (2000).

[20] L.-H. Yu and S. Krinsky, Nucl. Instrum. Methods Phys. Res., Sect. A **285**, 119 (1989).

[21] M. Xie, Nucl. Instrum. Methods Phys. Res., Sect. A **475**, 51 (2001).

[22] Z. Huang and K.-J. Kim, Nucl. Instrum. Methods Phys. Res., Sect. A **475**, 59 (2001).

[23] W. Fawley, Report Report LBNL-49625, LBL (2002).

[24] S. Reiche, Nucl. Instrum. Methods Phys. Res. A **429**, 243 (1999).

[25] E. Saldin, E. Schneidmiller, and M. Yurkov, Opt. Commun. **186**, 185 (2000).

[26] K.-J. Kim and Z. Huang, in *Proc. of the ICFA Beam Dynamics Workshop on the Physics of and Science with the X-ray Free-Electron Laser* (AIP, New York, 2001), no. 581 in AIP Conference Proceedings, p. 185.

[27] M. Zoloterov, private communications.

[28] R. Bonifacio, L. D. Salvo, P. Pierini, N. Piovella, and C. Pellegrini, Phys. Rev. Lett. **73**, 70 (1994).

[29] E. Saldin, E. Schneidmiller, and M. Yurkov, Opt. Commun. **148**, 383 (1998).

[30] L.-H. Yu, S. Krinsky, Nucl. Instrum. Methods Phys. Res., Sect. A **407**, 261 (1998).

[31] E. Saldin, E. Schneidmiller, and M. Yurkov, Opt. Commun. **212**, 377 (2002).

[32] P. Emma, K. Bane, M. Cornacchia, Z. Huang, H. Schlarb, G. Stupakov, and D. Walz, Phys. Rev. Lett. **92**, 074801 (2004).

[33] S. Krinsky and Z. Huang, Phys. Rev. ST Accel. Beams **6**, 050702 (2003).

[34] C. Schroeder, C. Pelligrini, S. Reiche, J. Arthor, and P. Emma, J. Opt. Soc. Am. B **19**, 1782 (2002).

[35] R. Bonifacio, L. D. Salvo, and P. Pierini, Nucl. Instrum. Methods Phys. Res., Sect. A **293**, 627 (1990).

[36] H. Freund, S. Biedron, and S. Milton, IEEE J. Quantum Electron. **QE-36**, 275 (2000).

[37] Z. Huang and K.-J. Kim, Phys. Rev. E **62**, 7295 (2000).

[38] W. Brefeld, B. Faatz, J. Feldhaus, M. Korfer, T. Moller, J. Pflueger, E. Saldin, E. Schneidmiller, J. Krzywinski, and M. Yurkov, Report 02-038, DESY (2002).

[39] Z. Huang and K.-J. Kim, Nucl. Instrum. Methods Phys. Res., Sect. A **475**, 112 (2001).

[40] N. A. Vinokurov, Z. Huang, O. A. Shevchenko, and K.-J. Kim, Nucl. Instrum. Methods Phys. Res., Sect. A **475**, 74 (2001).

[41] N. Kroll, P. Morton, and M. Rosenbluth, IEEE J. Quantum Electron. **QE-17**, 1436 (1981).

[42] S. Krinsky, Phys. Rev. E **69**, 066503 (2004).

[43] L.-H. Yu, S. Krinsky, R. Gluckstern, and J. van Zeijts, Phys. Rev. A **45**, 1163 (1992).

[44] T. Tanaka, H. Kitamura, and T. Shintake, Nucl. Instrum. Methods Phys. Res. A **528**, 172 (2004).

[45] K. Bane and G. Stupakov, Report SLAC-PUB-10707, SLAC (2004).

[46] Z. Huang and G. Stupakov, Phys. Rev. ST Accel. Beams **8**, 040702 (2005).

[47] K. Bane, P. Emma, W. Fawley, Z. Huang, H.-D. Nuhn, S. Reiche, G. Stupakov, this conference proceedings (2005).